



## OPEN ACCESS

## EDITED BY

Weijie Wang,  
China Institute of Water Resources and  
Hydropower Research, China

## REVIEWED BY

Dehai Song,  
Ocean University of China, China  
Busnur Rachotappa Manjunatha,  
Mangalore University, India

## \*CORRESPONDENCE

Barak Herut

✉ barak@ocean.org.il

Simona Avnaim-Katav

✉ simonaav@ocean.org.il

†These authors jointly supervised this work

‡Retired

RECEIVED 21 May 2023

ACCEPTED 18 September 2023

PUBLISHED 11 October 2023

## CITATION

Herut B, Guy-Haim T, Almogi-Labin A,  
Fischer HW, Ransby D, Sandler A, Katz T  
and Avnaim-Katav S (2023) Marine  
oligotrophication due to fine sediments  
and nutrient starvation caused by  
anthropogenic sediment and water  
retention in large rivers: the  
Nile damming case.  
*Front. Mar. Sci.* 10:1226379.  
doi: 10.3389/fmars.2023.1226379

## COPYRIGHT

© 2023 Herut, Guy-Haim, Almogi-Labin,  
Fischer, Ransby, Sandler, Katz and  
Avnaim-Katav. This is an open-access article  
distributed under the terms of the [Creative  
Commons Attribution License \(CC BY\)](https://creativecommons.org/licenses/by/4.0/). The  
use, distribution or reproduction in other  
forums is permitted, provided the original  
author(s) and the copyright owner(s) are  
credited and that the original publication in  
this journal is cited, in accordance with  
accepted academic practice. No use,  
distribution or reproduction is permitted  
which does not comply with these terms.

# Marine oligotrophication due to fine sediments and nutrient starvation caused by anthropogenic sediment and water retention in large rivers: the Nile damming case

Barak Herut<sup>1\*†</sup>, Tamar Guy-Haim<sup>1</sup>, Ahuva Almogi-Labin<sup>2†</sup>,  
Helmut W. Fischer<sup>3‡</sup>, Daniela Ransby<sup>4</sup>, Amir Sandler<sup>2</sup>,  
Timor Katz<sup>1</sup> and Simona Avnaim-Katav<sup>1\*</sup>

<sup>1</sup>Israel Oceanographic and Limnological Research, National Institute of Oceanography, Haifa, Israel,

<sup>2</sup>Geological Survey of Israel, Jerusalem, Israel, <sup>3</sup>Institute of Environmental Physics, University of Bremen, Bremen, Germany, <sup>4</sup>Alfred Wegener Institute, Helmholtz Centre for Polar and Marine Research, Bremerhaven, Germany

In the last two centuries, human activities have radically reduced the transport of suspended sediment and water to marine systems, mainly in the northern hemisphere, while complete sediment retention has been reported for the Nile River after the construction of the Aswan High Dam (AHD). Here, we focused on changes in the inner-shelf sediments most exposed to the pre-AHD flood plume in the distal part of its littoral cell as a predictor of the ecological response to large river fragmentation. Substantial reductions in fine (15–40%) and increases in coarse (~8 fold) sediment accumulation rates, increases in CaCO<sub>3</sub> (~50%), decreases in autochthonous and total organic carbon (OC), and changes in the benthic foraminiferal assemblage toward more OC-sensitive species suggest an enhanced oligotrophication trend. The reduced nutrient fluxes and OC accumulation, and the coarsening of the shelf sediments inhibit the retention of “blue” carbon. Combined with fast climate warming and salinization, river fragmentation may have essential implications for the Eastern Mediterranean ecosystem via benthic oligotrophication processes.

## KEYWORDS

nutrients, sediments, anthropogenic, dams, foraminifera, Mediterranean Sea, oligotrophic radionuclides

## 1 Introduction

Sediments and water transport by rivers have been dramatically changed by human activities in the last two centuries (Best, 2019), reducing their fluxes to the oceans mainly in the northern hemisphere (Syvitski et al., 2005; Dethier et al., 2022), or accelerating suspended sediment and fluxes in the southern hemisphere (south to 20° N) due to increased erosion resulting from intensive land use change (Dethier et al., 2022) and in high mountain Asia due to a warmer and wetter climate change (Li et al., 2021).

Dams and large reservoirs are responsible for extreme basin-wide sediment trapping in several rivers worldwide (Milliman and Farnsworth, 2013). Recent studies of pre- and post-damming in northern hemisphere rivers present a combined reduction in continental fluxes of  $49 \pm 25\%$ , while rivers with large dams are often intensively blocked (Milliman and Farnsworth, 2013; Dethier et al., 2022). An almost complete (~100%) trapping is reported for the Nile system (Vörösmarty et al., 2003; Syvitski et al., 2005; Milliman and Farnsworth, 2013). During the last two centuries, a series of dams have been built along the Nile, starting with the Aswan Low Dam (1898-1902), and since the operation of the Aswan High Dam (AHD; 1960-1964), almost all discharge to the southeastern (SE) Mediterranean Sea has been stopped, which includes  $\sim 10^7 \text{ t yr}^{-1}$  of fine sediments (Nixon, 2003), most of which is silty clay trapped in upper lake reservoirs (e.g., Lake Nasser) (Farhat and Salem, 2015). The Nile system shows severe fragmentation as compared to other major rivers in the world (Best, 2019) and has been subject to prolonged damming processes up to the most recent Grand Ethiopian Renaissance Dam (GERD, 2011-2020; Wheeler et al., 2020).

Prior to the AHD, the African monsoon caused extensive Nile River discharge/flooding into the Mediterranean Sea, averaging  $\sim 8 \times 10^{10} \text{ m}^3 \text{ yr}^{-1}$  (Sharaf El Din, 1977; Halim et al., 1995; Woodward et al., 2007; Rohling et al., 2015). Its reduced surface-water salinities and enhanced turbidity plume have been observed from the Nile Delta northward along the eastern Levantine coast (Hecht, 1964; Hecht and Gertman, 2001; Zviely et al., 2007). In the long past, the development of the East Mediterranean sapropels (sedimentary layers of high organic content) during the last ~13 million years has been linked to monsoon intensification and consequent discharge of the Nile as a major supplier of freshwater and suspended sediments to the basin, in addition to oceanographic pre-conditioning (Rohling et al., 2015). Since damming, Nile water discharge has been dramatically reduced (Sharaf El Din, 1977; Nixon, 2003; Ludwig et al., 2009), and seasonal monsoon-related floods (August-October) have stopped completely.

Sediment retention in reservoirs and the reduction of terrestrial sediment and water supply to coastal areas have a significant influence on coastal erosion, nutrient fluxes, the benthic shelf environment, and other marine resources (Stanley and Warne, 1993; Nixon, 2003; Syvitski et al., 2005; Abd-El Monsef et al., 2015). The area ratio between the Nile River drainage basin ( $2933 \times 10^3 \text{ km}^2$ ; Milliman and Farnsworth, 2013; Best, 2019) and the South Levantine marine basin ( $840 \times 10^3 \text{ km}^2$ ; Ludwig et al., 2009; Best,

2019) is exceptionally high (>3) compared to other large river-ocean system links, emphasizing its ideal relevance as a natural laboratory for assessing the impacts of fine sediment and nutrient retention by large, fragmented rivers on marine shelf ecosystems.

The combination of geochemical and faunal records can provide clues on benthic ecosystem changes. Benthic foraminifera (BF), living in marine shelf environments, are well-known single-celled eukaryotes highly sensitive to environmental changes. Their wide abundance and potential preservation in sedimentary archives make them ideal bioindicators for reconstructing past ecological, climatic, and anthropogenic changes (Jorissen et al., 1995; Sen Gupta, 1999; Katz et al., 2010; Avnaim-Katav et al., 2019; Schmiedl, 2019; Martínez et al., 2023), and they have recently been adopted as reliable indices for biomonitoring purposes (e.g., Bouchet et al., 2021). Furthermore, changes in BF species composition could be utilized as a reliable indicator of benthic macrofaunal community structure (Bouchet et al., 2018). Such recent (2011) changes in BF biotopes on the inner Mediterranean shelf off Israel, based on dissimilarities between the dead and live BF assemblages, were attributed to the long-term impacts of Nile damming (Avnaim-Katav et al., 2021).

The Nile system shows almost complete retention of fine sediments and nutrients that were transported to the SE Levantine Basin prior to the AHD, mimicking the marine consequences of severe fragmentation of large rivers worldwide. In this study, we focused on the distal part of the Nile littoral cell (Zviely et al., 2007) along the inner Mediterranean shelf off Israel (Figure 1) as a natural laboratory for a fast-responsive sedimentary system that has been affected by the Nile damming. Geochemical and sedimentological properties were analyzed in short sediment cores collected at 40 m water depth (Figure 1), representing the area of the pre-damming sedimentary silt belt (30-50m) (Nir, 1984) derived from past Nile floods that reach the Israeli coast at the end of each summer by wind-induced counterclockwise longshore currents (Hecht, 1964). In addition, to track benthic ecological changes attributed to the AHD, we analyzed BF assemblages in sedimentary layers representing pre- (~1910) and post- (1997; 2011; 2021) AHD conditions. The results show a substantial increase in grain size, a decrease in the organic carbon content and its marine/autochthonous fraction, and BF assemblages trending toward further oligotrophication.

## 2 Materials and methods

### 2.1 Field sampling

The presented data consist of a set of sediment samples obtained in this study and data from previous studies, as shown in Table 1. The data originate from short sediment cores and surface sediment samples collected along ~140 km of Israel's inner Mediterranean shelf from off Ashqelon in the south to off Beit Yannay in the north, representing the distal part of the Nile littoral cell at different periods (Figure 1; Table 1). The stations were located within the ~30-50 m water depth silty belt, an area most sensitive to past Nile River discharge/flood dynamics (Hecht, 1964; Nir, 1984).

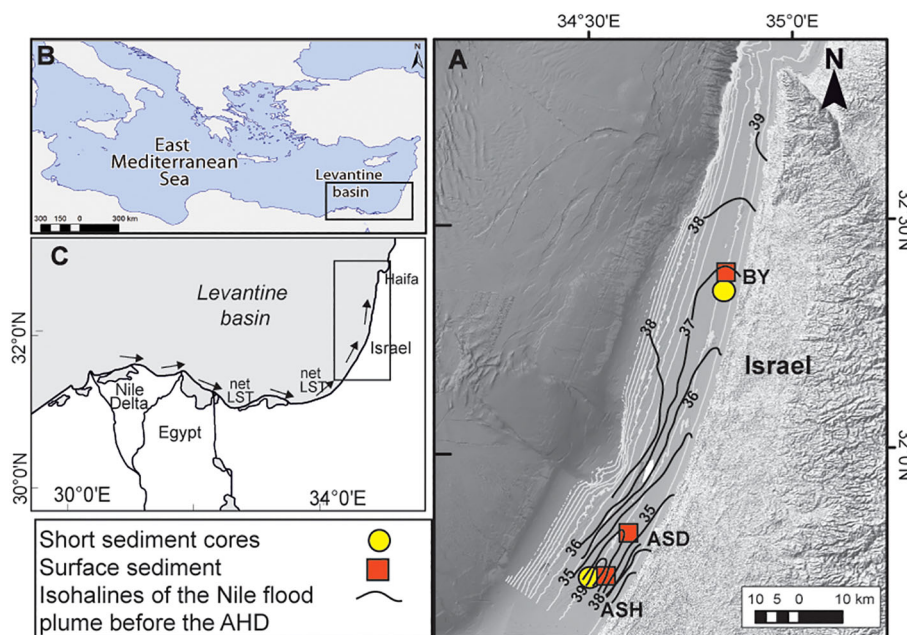


**FIGURE 1**  
 Locations of the studied short sediment cores (circles) (BY: 32°22.48N; 34°48.28E; ASH: 31°42.42N; 34°30.84E) and surface sediment box cores (boxes) (ASD: 31°47.86N; 34°32.20E) (A); Black contours are isohalines of the Nile flood plumes based on measurements before the Aswan High Dam (Hecht, 1964) (A). The Nile Delta (B, C) and the net long-shore transport (LST) flow northward along the SE Levantine basin coast off Israel (after Zviely et al., 2007) (C).

Short sediment cores were sampled in 2007 by the R/V *Shikmona* off Ashqelon (33 m water depth) and Beit Yannay (40 m water depth), representing the southern and northern zones of the study area. In addition, surface sediment samples were collected in 2021 by the R/V *Bat-Galim* at three stations (Ashkelon, Ashdod, and Beit Yannay) at ~40 m water depth. Surface sediments and the short cores were collected using a box corer (Ocean Instruments BX 700 AL, Ocean Instruments, Fall City, United States) and Perspex tubes.

The sediment cores were sliced onboard into 1 cm slices, frozen, and lyophilized in the laboratory. Sub-samples were analyzed for granulometry, major elements, CaCO<sub>3</sub>, P speciation, total organic carbon (TOC), and δ<sup>13</sup>Corg. Chronology was determined in two parallel cores using lead-210 (details are below).

Duplicates of surface sediment (top 0–1 cm) were sampled for micropaleontological analysis from each box core at each station. Because the abundance of living foraminiferal assemblages is low in the study area (Avnaim-Katav et al., 2020), each duplicate included three repeated samples of the top 0–1 cm interval using a 55 mm diameter Perspex mini corer. Micropaleontological analyses followed Schonfeld et al. (Schonfeld et al., 2012). Sediment samples were stained with rose bengal solution (2 g rose bengal/l 95%- ethanol) for two weeks at the time of sampling. Rose bengal confirms the presence of cytoplasm and is widely used to distinguish between dead and presumed live foraminifera (Avnaim-Katav et al., 2020; Avnaim-Katav et al., 2021). The samples for analyses of dead foraminiferal assemblages, representing pre-AHD deposition, were collected from the bottom layer of two short cores off Beit Yannay and Ashkelon.

**TABLE 1** Summary of the data set presented in this study.

Period	Sample type	Grain size	Geochemistry	Foraminifera	Locations	Reference
1900-2005	Short cores	+	+	Dead BF Abundance	Beit Yannay (BY); Ashkelon (ASH)	This study
1910 – pre AHD	Sediment bottom layers	+	Al, Si	Dead BF assemblage	Beit Yannay; Ashdod (ASD); Ashkelon	This study
1997	Sediment surface layers	+	+	Dead BF assemblage	Beit Yannay; Ashdod; Ashkelon	Hyams-Kaphzan et al. (2008)
2011	Sediment surface layers	+	+	Dead & Live BF assemblage	Beit Yannay; Ashdod; Ashkelon	Avnaim-Katav et al. (2020; 2021)
2021	Sediment surface layers	+	+	Dead & Live BF assemblage	Beit Yannay; Ashdod; Ashkelon	This study

## 2.2 Analytical methods

Grain size analysis followed [Crouvi et al. \(2008\)](#) and was performed on sediments <2 mm using a Malvern Mastersizer MS-2000 (Malvern Panalytical, Malvern, United Kingdom). Detailed information on the analysis of the major elements, Total Organic Carbon (TOC),  $\delta^{13}\text{C}$  of organic matter ( $\delta^{13}\text{C}_{\text{org}}$ ), and  $\text{CaCO}_3$  is presented in [Bookman et al. \(2021\)](#). In general, major elements were analyzed with an inductively coupled plasma-atomic emission spectrophotometer (ICP-OES OPTIMA 3300, Agilent Technologies, Santa Clara, United States) after the fusion of sediment sub-samples with  $\text{LiBO}_2$ . International standards (e.g., USGS SRS T-207, T-209) were used along with the known samples. The accuracy of the analyses of the major elements was better than 2%. Total Organic Carbon (TOC) content and  $\delta^{13}\text{C}_{\text{org}}$  were determined using the Thermo Flash 2000 Elemental Analyzer (manufactured by Thermo Fisher Scientific, Waltham, United States) that interfaced with a Thermo Finnigan Delta V Isotope Ratio Mass Spectrometer (IRMS) (Thermo Fisher Scientific) at the Geological Survey of Israel. The mass spectrometer measures the  $^{13}\text{C}/^{12}\text{C}$  ratio in the sample and standard and calculates the  $\delta^{13}\text{C}_{\text{org}}$  in ‰. All analyses have been reported relative to VPDB for  $\delta^{13}\text{C}_{\text{org}}$  and calibrated against the international standards Urea #2, Acetanilide #1, B2151, and B2153. The  $\text{CaCO}_3$  content was determined by gasometry.

P speciation was performed following [Eckert et al. \(2003\)](#) by sequential extraction of the solid phase to metal (Fe)-bound P. P bound to Fe hydroxides was released by leaching with NaOH (~0.1M) and measurement of molybdate-reactive P.

## 2.3 Chronology

The chronology of the two sediment cores was based on a combination of two radiotracers,  $^{210}\text{Pb}$  and  $^{137}\text{Cs}$ , due to their suitable half-lives of 22.2 and 30.0 years. A total of 38 slices of the sediment cores from ASH (19 upper 1 cm slices) and BY (19 upper 1 cm slices) were subjected to gamma spectroscopy. The dried sediments were sealed in cylindrical plastic dishes with a diameter of 3.5 cm using Rn-tight foil. Before measurement, they were left sealed for a minimum of 3 weeks so that the radioactive equilibrium between  $^{226}\text{Ra}$  and  $^{222}\text{Rn}$  (and their daughters) could be established.

For gamma spectroscopy, a coaxial HPGe detector with 50% relative efficiency (Canberra Industries/Mirion Technologies, Atlanta, United States) was used, housed in a 10 cm Pb shield with Cu and plastic inner linings, and operated under Genie 2000 software (Canberra Industries/Mirion Technologies). Measurement times varied from 77149 to 426623 seconds (long counting times of up to 5 days had to be used for samples with very low activity). Photopeak efficiencies were calculated using LabSOCS<sup>®</sup> (Laboratory SOURCEless Calibration System), the calibration tool of the Genie 2000 software (Mirion Technologies). The calculation is based on the definitions of sample geometry, composition and density, and sample-detector geometry, and the detector has been factory-characterized for use with LabSOCS. Comparison with

measurements of radioactive standard materials revealed deviations of less than 5% between measured and calculated efficiencies in most cases. The activity concentrations of all estimated radioisotopes were recalculated to the date of sampling. For the determination of  $^{210}\text{Pb}_{\text{xs}}$ , the excess  $^{210}\text{Pb}$  activity and the supported  $^{210}\text{Pb}$  activity (determined via the 351.9 keV line of  $^{214}\text{Pb}$ ) were subtracted from the total  $^{210}\text{Pb}$  signal, measured via the 46.5 keV line. Additionally, the artificial isotope  $^{137}\text{Cs}$  was analyzed via the 661.6 keV line of the daughter isotope  $^{137\text{m}}\text{Ba}$ . For several samples, no clear  $^{137}\text{Cs}$  signal could be detected at the 95% confidence level. The decision threshold varied for individual samples, mainly depending on their mass and counting time, and mostly reached values between 0.4 and 1.0  $\text{Bq kg}^{-1}$ . The chronological models were applied to data expressed in units of activity concentration  $\text{Bq kg}^{-1}$ . Comparable results (within standard error) were obtained with data recalculated to  $\text{Bq cm}^{-3}$  using dry densities that do not vary significantly in the profiles. A grain size normalization procedure was applied to the  $^{210}\text{Pb}_{\text{xs}}$  data ([Kirchner and Ehlers, 1998](#)). When  $^{210}\text{Pb}_{\text{xs}}$  and  $^{137}\text{Cs}$  enter the marine environment, they are removed from the solution by adsorption on inorganic particles or organic matter in suspension, which is later deposited on the bottom. Most of the activity is linked to the finest fraction with the highest effective surface area. The sediment cores were dated by applying a simple exponential model (constant  $^{210}\text{Pb}_{\text{xs}}$  flux, constant sedimentation rate) to normalized data from the profiles ([Supplementary Figure 1](#)). Variations in sediment particle size were accounted for using the fine fraction for grain size correction ( $^{210}\text{Pb}_{\text{xs}}$  ( $\text{Bq kg}^{-1}$ )/fraction <63  $\mu\text{m}$  (%) \* 100). When alternatively using Al content ([Alvarez-Iglesias et al., 2007](#)) for fine material normalization ( $^{210}\text{Pb}_{\text{xs}}$  ( $\text{Bq kg}^{-1}$ )/Al (%) \* 100, data not shown), the data look very similar to those after grain size correction. We confirmed this by the appearance of the  $^{137}\text{Cs}$  values and the geochemical profiles, which support this sedimentation model and the pre-1950s origin of the deeper layers. The accompanying radionuclide data and age model can be found in the PANGAEA data repository ([Ransby et al., 2023](#)).

## 2.4 Foraminiferal analysis

In total, 55 surface and sub-surface sediment samples were washed through a 63  $\mu\text{m}$  sieve and dried at 50°C, and the >125  $\mu\text{m}$  fraction was used for foraminiferal analyses ([Table 1](#)). The living assemblage, which included individuals with bright pink and homogeneous cytoplasm, was studied in the entire duplicate sample according to the protocol of [Schonfeld et al. \(2012\)](#). The living assemblage in all of these samples (except for three samples with <50 specimens) had more than 100 individuals, a sufficient number for multivariate statistical methods, and relatively robust environmental interpretation ([Hayward et al., 2019](#)). The time-averaged dead assemblage in recently deposited sediments (2021) and pre-AHD dam samples was examined in samples that were split into aliquots containing generally at least 200 dead specimens (one-quarter of the samples contained 118 to 166 shells, and the remaining contained 217 to 590 shells). Specimens were identified

to species level and counted to determine the total number of benthic foraminiferal individuals per gram of dry sediment (BF/g). Taxonomic identification was based on [Loeblich and Tappan \(1987; 1994\)](#); [Cimerman and Langer \(1991\)](#); [Hottinger et al. \(1993\)](#); [Jones \(1994\)](#), and the World Foraminifera Database, [World Register of Marine Species \(2023\)](#). The state of preservation of the specimens was evaluated and was generally very good in all samples examined.

## 2.5 Statistical analysis

To measure the differences in community structure between study periods and study sites in the live and dead assemblages, we performed non-metric multidimensional scaling (NMDS) ordinations after computation of a Bray-Curtis dissimilarity matrix based on foraminifera abundances using the “vegan” package (version 2.5-6) ([Oksanen et al., 2019](#)) in R v4.2.2 (R Core Team, 2021). Foraminiferal abundance data were  $\log(x+1)$  transformed prior to analyses to reduce the influence of the most abundant species. As an additional test, we performed Ward.D hierarchical cluster analysis on the Bray-Curtis dissimilarity matrix using the `hclust` function in the “vegan” package. The Ward.D algorithm is based on minimizing variances in hierarchically identified assemblages and fits aggregated data, for which the Bray-Curtis measure is generally recommended ([Singh et al., 2011](#)). Transformed abundances and clustering were visualized using the “pheatmap” package in R ([Kolde and Maintainer, 2018](#)). The significance of the differences between live and dead foraminiferal assemblages derived from the Bray-Curtis matrix was assessed with PERMANOVA (permutational multivariate ANOVA) tests, with period and site as fixed factors, followed by *post-hoc* pairwise comparisons. We further calculated the relative contribution of each species to the similarities within each assemblage using a SIMPER (similarity percentage) analysis, which examines the percentage contribution of each species to the similarity within and dissimilarity between assemblages ([Clarke, 1993](#)).

Following the classification of benthic foraminifera into five categories based on their ecological quality status (EcoQS) ([Alve et al., 2016](#)), we have analyzed the temporal changes in the total relative abundance of category 1 (oligotrophic bioindicators) and category 3 (eutrophic bioindicators) using the Kruskal-Wallis rank sum test in R.

## 3 Results and discussion

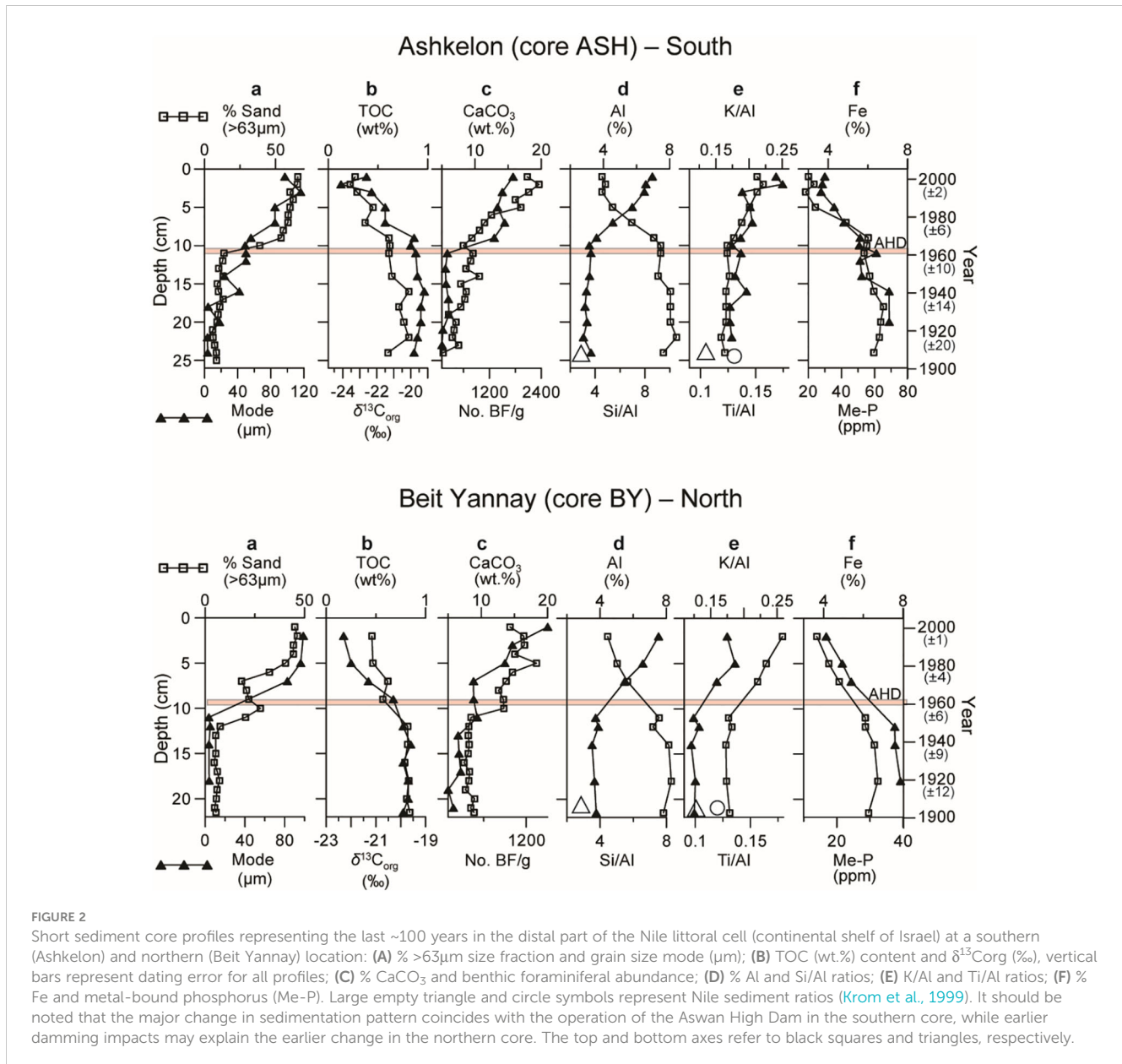
The Israeli inner continental shelf is an integral and distal part of the Nile littoral cell, extending ~700 km from Alexandria, Egypt, in the south, to Akko, Israel, in the north ([Inman, 2003](#); [Zviely et al., 2007](#)). Prior to the AHD, the Nile flood events in late summer (between August and November) discharged approximately 50% of the flood volume into the Mediterranean Sea, estimated to be  $\sim 84 \times 10^9 \text{ m}^3$  between 1900 and 1959 and  $\sim 55 \times 10^9 \text{ m}^3$  between 1959 and 1963 ([Halim et al., 1995](#)). These annual floods produced a plume of turbid (brownish) water that transported nutrients and

$\sim 117 \text{ t/y}$  of fine sediments along the shallow coastal water towards the distal part of the Nile littoral cell off Israel ([Oren and Komarovsky, 1961](#); [Hecht, 1964](#); [Oren, 1969](#); [Sharaf El Din, 1977](#); [Halim et al., 1995](#)). Sediments from the Nile River and the submerged delta were transported to the east by the prevailing waves and the wind-induced counterclockwise longshore currents ([Inman and Jenkins, 1984](#); [Inman, 2003](#)). The effect of the late summer Nile flood events was dramatic, recording a drop-in in salinity (from 39 to as low as 33 psu), an increase in turbid nutrient-enriched waters and phytoplankton biomass, and a change in the phytoplankton composition of the surface waters ([Halim, 1960](#); [Oren and Komarovsky, 1961](#); [Hecht, 1964](#)). Below, we show that the sediment regime of the inner shelf of Israel has indeed recorded the dramatic impact attributed to the prevention of the Nile flood discharge, both of suspended particulate matter and nutrient-induced organic matter, pioneering at the distal part of its littoral cell. This damming process terminates a long climatological Nile-derived geological record of changing flow intensities affecting the SE Levantine sedimentary province ([Bookman et al., 2021](#)) and the eastern Mediterranean basin in general ([Rohling et al., 2015](#)).

### 3.1 Impact of the Aswan High Dam on the geochemical properties and organic matter sources of the distal Nile littoral cell

Here, we present the geochemical changes in two short sediment cores, one located at the northernmost edge of the Nile littoral cell (BY) and the other ~100 km to the south (ASH), assuming that they best represent the outcomes of the Nile damming. Indeed, the top ~10 cm, accumulated during the last ~40 years, is significantly coarser than the underlying pre-AHD sediments ([Figure 2A](#)).

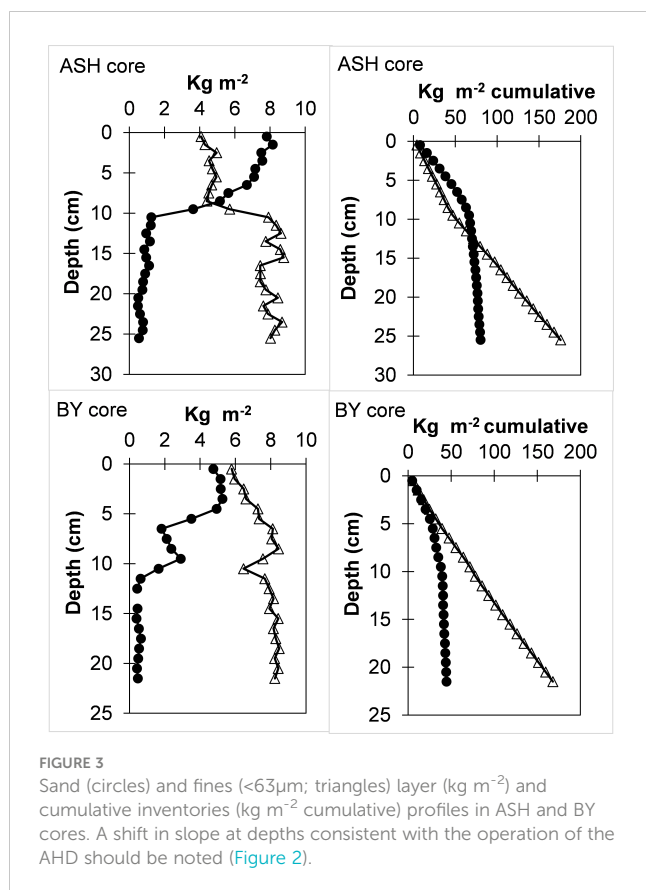
Applying the exponential model to the grain size normalized data in cores ASH and BY, we obtained sedimentation rates of  $2.3 \pm 0.5 \text{ mm yr}^{-1}$  and  $1.8 \pm 0.3 \text{ mm yr}^{-1}$ , respectively. The occurrence of  $^{137}\text{Cs}$  at the depths of 10.5 cm and ~7 cm in cores ASH and BY, respectively, was thus dated to 1962 ( $\pm 10 \text{ yr}$ ) and 1967 ( $\pm 7 \text{ yr}$ ), respectively, in good agreement with the maximum of the  $^{137}\text{Cs}$  bomb test fallout in 1963 ([Supplementary Figure 1](#)).  $^{137}\text{Cs}$  is associated with organic matter and the fine clay mineral fraction in sediments, which makes its detection analytically easier in fine-grained, organically rich sediment types. The fact that no  $^{137}\text{Cs}$  could be detected in the deeper, finer layers, while it was detected with the same experimental setup in the coarser sediments in the shallower layers, strongly supports the pre-1950s origin of the deeper layers. Extrapolation of the  $^{210}\text{Pb}$ -derived sedimentation rate to depths beyond 10 cm is somewhat uncertain, as the data scatter is very large. On the other hand, for both cores, the  $^{210}\text{Pb}$  inventory in the upper 10 cm corresponds to about 75% of the total inventory ( $1305$  of  $1756 \text{ Bq m}^{-2}$  for ASH,  $3350$  of  $4033 \text{ Bq m}^{-2}$  for BC), which also supports the assumption that these sections are not much older than two half-lives of the radioisotope, i.e., approximately 45 years. Although it cannot be excluded from the data that  $^{210}\text{Pb}$  is present at depths below 20 cm that are not accessible in this data set, the ratio of inventories above and below



10 cm is a strong argument for the age model and its extrapolation to greater depths.

Analysis of the normalized sand and fines (<63µm) inventories in the two cores ( $\text{kg m}^{-2}$ ; considering the porosity and particle density of  $2.65 \text{ gr cm}^{-3}$ ) shows a shift at depths that correspond to the mid-1960s, post-AHD, according to the  $^{210}\text{Pb}$  exponential age model (Figure 3). The sedimentation rates and the slope of the cumulative sands and fines (Figure 3) were used to calculate the mean annual accumulation along the cores. Accordingly, for the BY core, we calculated mean sand and fines accumulation rates of  $0.08$  and  $1.5 \text{ kg m}^{-2} \text{ y}^{-1}$  before the mid-1960s and  $0.66$  and  $1.3 \text{ kg m}^{-2} \text{ y}^{-1}$  thereafter, respectively. For the ASH core, mean sand and fines accumulation rates were  $0.2$  and  $1.9 \text{ kg m}^{-2} \text{ y}^{-1}$  before the mid-1960s and  $1.6$  and  $1.1 \text{ kg m}^{-2} \text{ y}^{-1}$  thereafter, respectively. This would indicate a respective ~15% and ~40% reduction in fines accumulation rates in BY and ASH cores, respectively, and an ~8-

fold increase in sand accumulation rates in both stations. A certain increase in the sand fraction (coarsening) in the top layers would occur solely from the decrease in the flux of Nile-derived fine sediments while maintaining the sand flux as in the previous AHD. Nonetheless, these unexpected calculated accumulation rates suggest that sand transport increased from the Nile Delta northward to the inner shelf band of Israel after the AHD. This estimate holds even if, for some unknown reason, our age model grossly (e.g., by a factor of four) overestimated post-AHD sedimentation rates. A possible cause for such a process is probably associated with the accelerated erosion rates of the sandy Nile Delta (tens of meters per year) after the AHD (3-5 times the rates before the AHD) and the northeastward transport and export of these sands along the coast (Frihy, 1988; Smith and Abdel-Kader, 1988; Frihy and Komar, 1991; Inman et al., 1993; Frihy and Lotfy, 1997). It has been proposed that the blockage of the



blockage of the Nile sand caused by the AHD forced currents to remove sand from the delta coast, compensating for the reduction and preventing sand shortages further north in the Nile littoral cell (Zviely et al., 2007). Additionally, man-made structures such as breakwaters in ports in Egypt, Gaza, and Israel may have diverted transported sand further offshore. Other factors that may somewhat affect sediment transport and grain size distribution on the shelf may include extreme flooding of the large ephemeral El-Arish River (Klein, 2000), fluctuations in erosion rates of the coastal escarpment (Mushkin et al., 2016), and various physical processes (Van Wellen et al., 2000; Shaeri et al., 2020).

The sand content exceeds  $\sim 50\%$  in the post-AHD sediments, compared to  $<20\%$  in the pre-AHD sediments (Figure 2A). The grain size mode increased gradually from  $\sim 5\ \mu\text{m}$  in the pre-AHD sediments to  $\geq 85\ \mu\text{m}$  in the post-AHD sediments. The silt fraction, which was  $\sim 75\%$  in the pre-AHD sediments, decreased to  $\sim 45\%$  in the post-AHD sediments, and the clay content decreased by  $\sim 50\%$ , from  $\sim 20\%$  to  $<10\%$ . The latter reduction in fine sediments post-AHD is reflected in the changes in the chemical composition of the sediments, which show significantly higher Al and Fe concentrations and lower Si/Al ratios in the pre-AHD sediments (Figures 2D, F). The significantly lower K/Al, Ti/Al, and Si/Al ratios in the pre-AHD shelf sediments (Figures 2D, E) coincide with these ratios in the Nile sediments (Krom et al., 1999), emphasizing their strong reduction in the post-AHD sediments. Sediment coarsening is also accompanied by a distinct but moderate increase in  $\text{CaCO}_3$ , from less than 10% to 15–20%, mainly attributed to the increase in BF abundance (Figure 2C). The grain size coarsening is more abrupt

and rapid in the southern shelf (ASH core), closer to the Nile, than in the northern distal part (BY core; Figure 2). In the latter, the coarsening starts earlier, is more gradual, and increases in two steps, probably in response to an earlier stage of Nile damming (since the Aswan Low Dam in 1898–1902) that was barely recorded in the southern shelf.

TOC contents of 0.8–1wt.% with  $\delta^{13}\text{C}_{\text{org}}$  of approximately  $-19.5\text{‰}$  in pre-AHD sediments decreased to less than 0.5wt.% TOC and approximately  $-22\text{--}23\text{‰}$   $\delta^{13}\text{C}_{\text{org}}$  in the overlying younger sediments (Figure 2B). Metal (mainly iron oxides)-bound phosphorus concentrations are lower in the post-AHD sediments, probably reflecting reduced scavenged phosphate in iron oxides as compared to the enhanced discharge of nutrients and iron in the pre-AHD period, especially during the seasonal floods (Figure 2F).

The bulk geochemical data from the two sediment cores are presented in Supplementary Table 1. Processing the geochemical data for principal component analysis (PCA) reveals two principal components that account for approximately 94% of the total variance in both sediment cores. Supplementary Figure 2 shows that the variance in elemental composition corresponds to the relative contribution of two major sources: terrestrial and marine-biogenic. The marine component contributes mainly to Ca or  $\text{CaCO}_3$  as a major constituent of micro- and macro-faunal shells and to Si as a major constituent of quartz grains, both of which affect the proportion of sand grain size. Al, Fe, Mg, K, and Ti mostly correspond to terrestrial aluminosilicate minerals. Metal (mainly iron oxides)-bound phosphorus (P-metal) concentrations are linked to terrestrial sources of both dissolved phosphate and iron. The variance of TOC and its isotopic composition seem predominantly affected by the change in the terrestrial discharge of dissolved nutrients that trigger the marine-born TOC.

The relationships between  $\delta^{13}\text{C}_{\text{org}}$  and TOC (Figure 4) show a mixing curve between depleted TOC with relatively more negative  $\delta^{13}\text{C}_{\text{org}}$  in the post-AHD period and a more enriched TOC with a marine/algae  $\delta^{13}\text{C}_{\text{org}}$  signature in the pre-AHD sediment. The  $\sim 3\text{‰}$  decrease ( $-19.2$  to  $-22.6\text{‰}$ ; one measurement of  $-24.6\text{‰}$ ; Figure 4) in  $\delta^{13}\text{C}_{\text{org}}$  may reflect a shift in the relative contribution of autochthonous versus allochthonous organic carbon. Marine planktonic  $\delta^{13}\text{C}$  in the eastern Mediterranean and other marine areas at similar latitudes ranges between  $-18$  and  $-22\text{‰}$  (Goericke and Fry, 1994; Meyers, 1994; Harmelin-Vivien et al., 2008; Li et al., 2016), and terrestrial  $\delta^{13}\text{C}$  ranges from  $-25$  to  $-28\text{‰}$  (Hedges et al., 1997; Li et al., 2016). The  $\sim 50\%$  decrease in TOC may indicate a drastic reduction in dissolved nutrient supply post-AHD. This observation suggests that prior to the AHD, the Nile system supplied significant amounts of dissolved nutrients to its distal cell, which enhanced algal biomass and the sedimentation of autochthonous organic carbon, but only an insignificant amount of allochthonous organic carbon. While the pre-AHD transported significant amounts of silty-clay sediments, it is speculated that the Nile-born detrital organic matter was decomposed or retained in the Nile delta, while the dissolved nutrients, representing a much larger stock, were transported northward along the eastern Levantine coast, fueling the primary producers, especially during the seasonal floods. The floods peaked between August and October/November (Sharaf El Din, 1977) and triggered a large

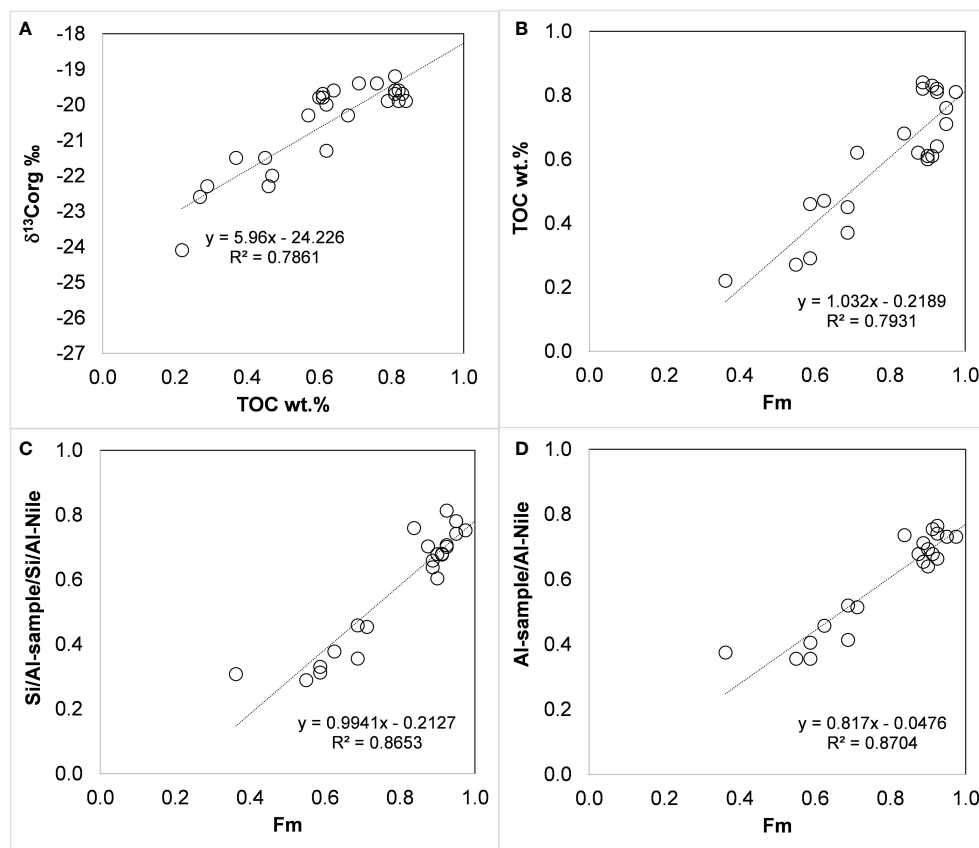


FIGURE 4

$\delta^{13}\text{C}_{\text{org}}$  ‰ vs. TOC % (A), TOC % vs. marine fraction (Fm, eq. 2) (B), [Si/Al-sample]/[Si/Al-Nile] vs. Fm (C), and [Al-sample/Al-Nile] vs. Fm (D). [Si/Al-Nile] = 2.483 wt./wt. and [Al-Nile] = ~11 wt.% (Krom et al., 1999).

phytoplankton bloom in the nearshore waters off the Egyptian and Israeli coasts (Oren and Komarovskiy, 1961; Dowidar, 1984). At present, the southeastern Mediterranean Levantine Basin and coastal waters off Israel display oligotrophic conditions (Herut et al., 2000; Kress et al., 2019). Nonetheless, partial, but probably not dominant, changes in the TOC content can be attributed to the significant increase in grain size after the AHD (Hedges and Oades, 1997; Magill et al., 2018).

The changes in  $\delta^{13}\text{C}_{\text{org}}$  composition in shallow continental shelf sediments are a first-order estimate due to mixing between marine/autochthonous and terrestrial/allochthonous organic carbon (Shultz and Calder, 1976). The isotopic mixing equation then represents a conservative mixing of these two end members (Shultz and Calder, 1976):

$$\delta^{13}\text{C}_{\text{org}} - \text{sample} = F_m \times \delta^{13}\text{C}_{\text{org}} - m + F_t \times \delta^{13}\text{C}_{\text{org}} - t \quad (1)$$

where  $F_m$  and  $F_t$  are the fractions of marine and terrestrial organic carbon ( $F_m + F_t = 1$ ), and  $\delta^{13}\text{C}_{\text{org}} - m$  and  $\delta^{13}\text{C}_{\text{org}} - t$  are the isotopic compositions of the terrestrial and marine source end members.

Rearranging Equation 1,

$$F_m = [\delta^{13}\text{C}_{\text{org}} - \text{sample} - \delta^{13}\text{C}_{\text{org}} - t] / [\delta^{13}\text{C}_{\text{org}} - m - \delta^{13}\text{C}_{\text{org}} - t] \quad (2)$$

Based on the above literature data, we calculated  $F_m$  (eq. 2) using a terrestrial  $\delta^{13}\text{C}_t$  of -27 ‰ and  $\delta^{13}\text{C}_{\text{org}} - m$  -19 ‰ as end members.  $F_m$  ranges from 0.4 to ~0.9 before the AHD, corresponding to higher TOC concentrations. We assumed that the Si/Al or Al ratios between the sample and the Nile sediment end member (Si/Al ratio of 2.483 wt./wt. and Al concentration of ~11 wt.%; Krom et al., 1999) could serve as a proxy for the intensity of dissolved nutrient supply, as they coincide with the transport of Nile-derived fine sediments. These ratios may represent the fraction of marine-born organic carbon attributable to the supply of Nile-derived nutrients, as they show a similar fractional range and a significant linear correlation with  $F_m$  calculated from carbon isotopic composition (Figure 4).

The decline in these variables reflects a major change in the regional nutrient budget and a large decrease in primary production that coincides with the damming of the Nile (Halim et al., 1995). The trend of increasing oligotrophy on the inner shelf of Israel differs from reports of a large anthropogenic contribution of nutrients supporting increasing fisheries in the Mediterranean coastal waters off Egypt (Nixon, 2003). This increase in fertility seems to be on a local scale, mainly restricted to the delta area, unlike the pre-AHD summer floods, which were of significant and large magnitude and affected the Israeli shelf annually. The decrease

in TOC and  $\delta^{13}\text{C}_{\text{org}}$ , indicators of nutrient supply and primary production, predates the sharp sediment coarsening. This may indicate that earlier phases of Nile damming had already contributed to the increasing oligotrophy of the EM, which accelerated after the operation of the AHD and continues at present.

### 3.2 Changes in the dead and live foraminiferal assemblages as proxies for the ecological evolution attributed to the damming of the Nile

The current study traces the temporal variations in the BF assemblage composition linked to changes in the sedimentary regime in the distal part of the Nile littoral cell following the damming of the Nile. We presented the BF assemblages in sedimentary layers representing pre (~1910) and post (1997; 2011; 2021) AHD conditions. The integrated database of surface and subsurface sediment samples (Table 1) contains a total of 170 taxa, of which 120 were identified at the species level after taxonomic refinement (Supplementary Table 2). The comparison of species accumulation curves of 10 surface sediment samples collected in 2021 between BY and ASH stations (three versus five sites) indicates that the three chosen sites represent 92% of the total species richness (56/61 species) (Supplementary Table 3; Supplementary Figure 3).

Cluster analysis and nonmetric multidimensional scaling (NMDS) ordination revealed a clear separation between dead (cluster A) and live (cluster B) BF assemblages and time periods, as detailed below (Figure 5; Supplementary Figure 4; Supplementary Table 4, Permanova analysis). We focused mainly on the dead BF assemblage, which provides the long-term record since before the AHD and integrates time-averaged information. The dead BF (Cluster A, Supplementary Figure 4) are divided into two major sub-clusters, A1 and A2, which are further subdivided by periods. A1 includes the separation between pre-AHD and 1997 samples, and A2 shows the division between 1997, 2011, and 2021 (Figure 5). Pairwise analysis between periods showed a significant difference ( $p < 0.02$ ) between pre-AHD, 2011 and 2021, and between 1997, 2011, and 2021 (Supplementary Table 5). The opportunistic species *Ammonia tepida*, *Porosonion subgranosus*, and *Criboelphidium poeyanum* are among the most significant species in the pre-AHD samples (in sub-cluster A1), contributing 35% of the similarity between these samples (SIMPER, Supplementary Table 6). Their relative abundances ranged between 21–42%, 4–22%, and 8–18% of the assemblage composition, respectively. While these species may inhibit sediments poor in TOC, their highest abundances are favored by organic carbon enrichment (e.g., Bouchet et al., 2018; Jorissen et al., 2018). These species are also part of the 1997 samples; however, their contribution is relatively much lower, while other species such as *Ammonia parkinsoniana*, *Asterigerinata mamilla*, and *Textularia agglutinans* show increased relative abundances, ranging between 3–7%, 4–14% and 2–3%, respectively. These latter

species are known to be sensitive to organic carbon enrichment and occur mainly in natural oligotrophic ecosystems (Alve et al., 2016; Jorissen et al., 2018).

We used the classification of ecological groups following Bouchet et al. (2021) as a proxy for changes in sedimentary total organic carbon levels. Based on the ecological quality status (EcoQS) BF groups, the two most relevant categories for changes in the Nile damming sediments are category 1 (sensitive species - oligotrophic bioindicators) and category 3 (tolerant species to organic carbon enrichment - elevated trophic state bioindicators). EcoQS category 1 showed an increasing trend over time ( $p < 0.02$ ; Kruskal-Wallis rank sum test), while category 3 showed significantly lower levels during 1997–2021 than in the pre-AHD (Figure 6; Supplementary Table 7). These trends are consistent with the geochemical observations showing lower TOC and fine sediment post-AHD.

EcoQS category 2 includes “indifferent species” to organic carbon enrichment, which are usually observed at relatively low abundances (Bouchet et al., 2021). It is thus expected that this group will be less responsive to the inferred damming effects and the decrease in TOC, as indeed observed along the periods (Figure 6). They occur in low abundance, with no changes between the different periods.

Additionally, based on pairwise analyses, the similarity between sites within periods showed that in pre-AHD and 1997, the BY station was the most dissimilar to the ASH and ASD stations ( $p < 0.04$ , Permanova, Supplementary Table 8), while in 2011–2021, a greater dissimilarity developed between the two southern stations (ASH and AHD). This spatial dissimilarity trend suggests a further ongoing process from the northernmost distal part of the Nile cell southward.

Although live BF populations represent a snapshot of seasonal distribution that may record taphonomic processes compared to the subsurface assemblages, they are also responsive to anthropogenic impacts (e.g., Kidwell, 2007; Goineau et al., 2015). Indications for the ongoing changes in the BF composition associated with the damming of the Nile are also recorded in the live BF communities collected in 2011 and 2021. *Eggerelloides scaber*, *Paratrochammina madeira*, and the sensitive species *Bolivina striatula*, *Cycloforina quinquecarinata*, and *Textularia agglutinans* are among the living BF that contribute most (60% contribution) to the similarity between the samples of cluster B, based on SIMPER (Figure 5; Supplementary Table 6). EcoQS category 1 showed a slight decrease (of about 10%) in their abundance compared to their appearance in the dead assemblages of 2020 (Figure 6), while category 3 of opportunistic species continued to decrease in their density, representing 4% of the assemblage. The ongoing changes in sediment properties demonstrate the continuous impact of the Nile damming and the subsequent enhanced benthic oligotrophication process. Changes in the composition of the live BF assemblage have been observed over the last two decades on the southeastern Mediterranean shelf, where the Nilotic biotope has retreated southward (Avnaim-Katav et al., 2020; Avnaim-Katav et al., 2021). We speculate that the ongoing environmental changes in this unique ecosystem will continue to affect the distribution of benthic communities along the shelves of the Nile domain and thus require further study.

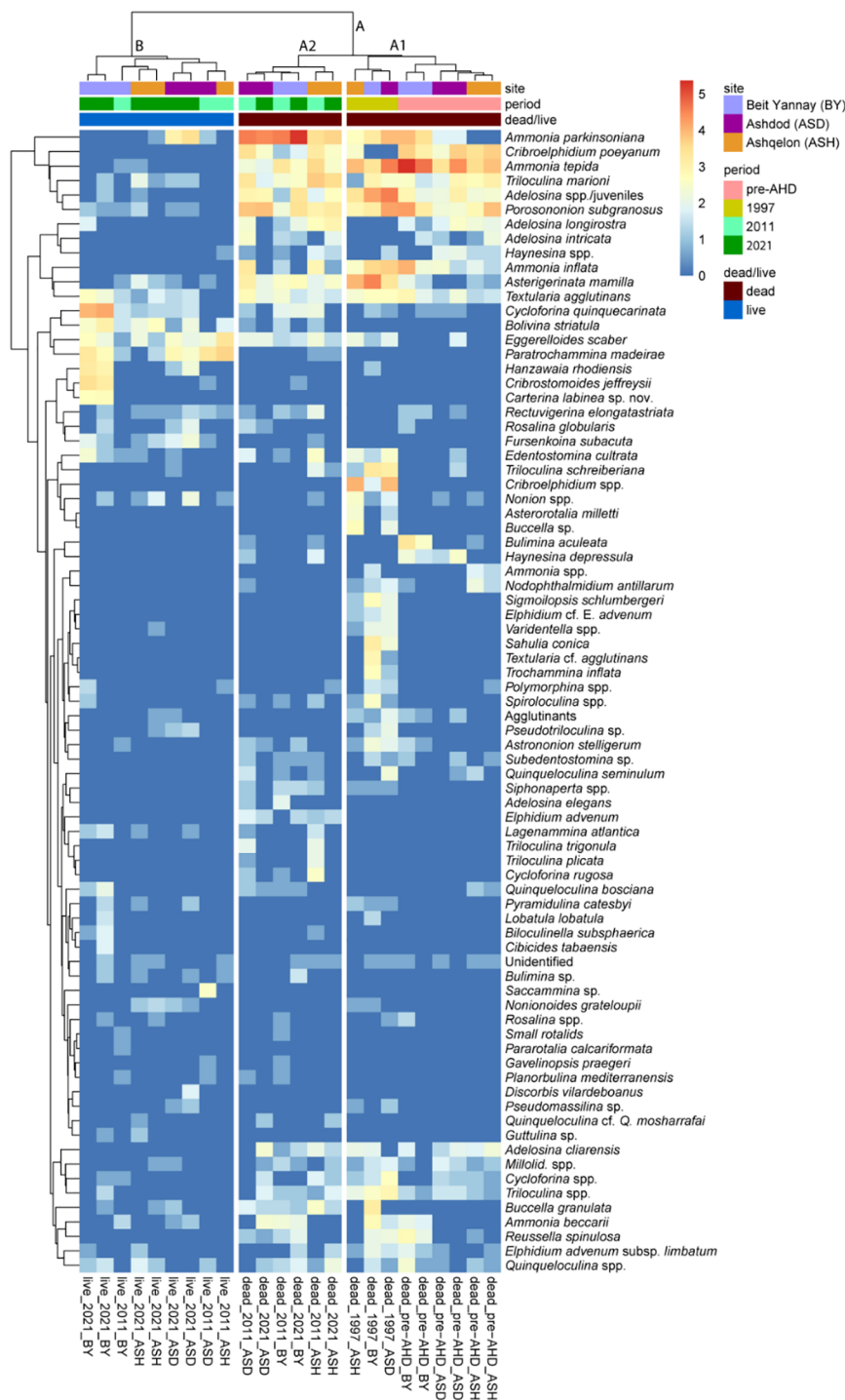


**FIGURE 5** Q-mode Ward.D hierarchical cluster analysis of the surface and subsurface samples from stations BY, ASH, and ASD on the southeastern Mediterranean shelf (40 m water depth), representing the pre-AHD, 1997, 2011, and 2021 periods. The figure presents a visualization of the relative proportions of the 101 major taxa (>2% of the total assemblage) contributing to the clusters. The cluster analysis and the heat map of the full dataset of 170 taxa are shown in [Supplementary Figure 4](#). A clear separation between dead (cluster A) and live (cluster B) BF assemblages and time periods (sub-clusters A1 and A2) is highlighted.

## 4 Conclusion

In this work, we followed the benthic sedimentological changes during the last approximately 100 years, which were significantly

influenced by the damming of the Nile River, resulting in an almost complete retention of fine sediments and a decrease of dissolved nutrients previously exported to its distal domain in the southeastern Mediterranean basin. The substantial change in

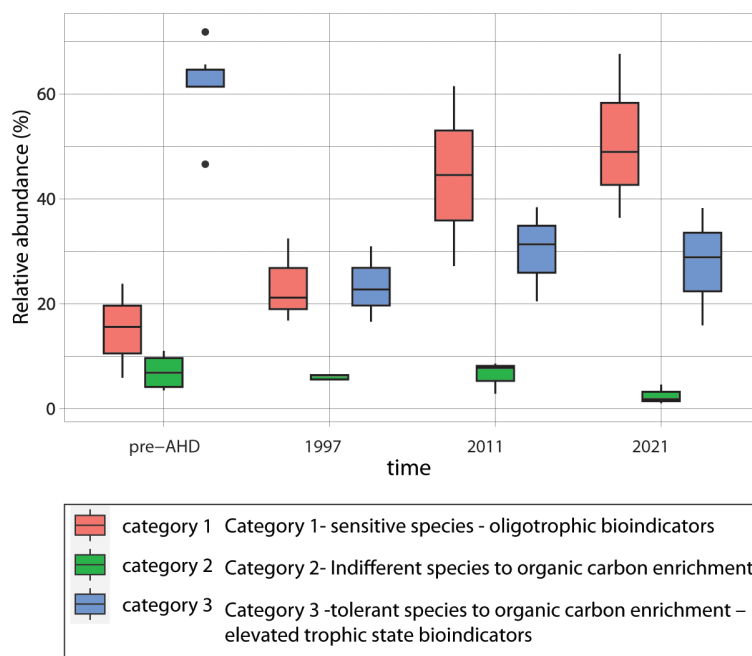


FIGURE 6

Box plots of BF ecological groups following Bouchet et al. (2021) as a proxy for changes in the sedimentary total organic carbon levels. Three BF ecological quality status (EcoQS) groups are presented for the different time periods: category 1 - sensitive species (oligotrophic bioindicators), category 2 - "indifferent species", and category 3 - tolerant species to organic carbon enrichment (elevated trophic state bioindicators).

grain size, organic carbon, and BF assemblages, tending toward further oligotrophication, combined with fast warming and salinization in the Levantine basin (Ozer et al., 2022), mainly attributed to climate change, may have essential implications for the southeastern Mediterranean ecosystem. The assessment of the effects of climate change on the nutrient dynamics and the planktonic ecosystem in the western and eastern basins of the Mediterranean Sea is mostly based on the analysis of simulations under different Representative Concentration Pathways (RCPs) 4.5 and 8.5, as presented by Reale et al. (2022) and references therein. While different projections have been reported, Reale et al. (2022) show stable nutrient concentrations in the euphotic layer until 2030 and a significant decrease thereafter for the worst-case scenario (RCP8.5). Nevertheless, the projection of the biogeochemical/nutrient responses to river loading and Gibraltar exchange associated with climate change is highly important and requires further investigation (Richon et al., 2019). While in this study the damming of the Nile is evident by the turnover observed in the foraminiferal species composition shifting from EcoQS category 3 to EcoQS category 1 (Figure 6), the global warming trend is likely to alter the BF assemblages on the continental shelf, but further research is needed to follow this effect.

Both the reduced nutrient fluxes and the coarsening of the shelf sediments may reduce the preservation of organic matter and the retention of "blue" carbon in the shelf sediments. The severe fragmentation of the Nile and other coastal river systems may also interrupt the past periodic formation of sapropels (rich organic layers) over the last 13.5 million years, known from sedimentary sequences in the eastern Mediterranean basin, corresponding to monsoon runoff/intensification and other oceanographic

preconditions (Rohling et al., 2015). The Nile system may serve as a predictor of ecological marine responses in other large, fragmented rivers worldwide where human activities have significantly reduced their sediment and water fluxes (Syvitski et al., 2005; Best, 2019; Dethier et al., 2022).

## Data availability statement

The original contributions presented in the study are included in the article/Supplementary Material, further inquiries can be directed to the corresponding author/s.

## Author contributions

Conceptualization: BH and AA-L; Sampling: BH, AA-L, and TK; Methodology: AA-L, BH, TK, TG-H, AS, and SA-K; Chronology: HF and DR; Statistics: TG-H; Writing-original draft: BH and SA-K; Writing and editing: All authors participated in discussion and writing; Resources: BH and AA-L. All authors contributed to the article and approved the submitted version.

## Funding

This study was carried out with the support of the Israeli Ministry of Energy (grant no. 28-17-006), partially by the Israel Science Foundation (grant 145/02-13.0) to AA-L and BH, and partially by the National Monitoring Program of Israel's Mediterranean Waters.

## Acknowledgments

We would like to thank the team of the geochemical and sedimentological units of the Geological Survey of Israel for their help in sampling and analysis; we thank the chemistry laboratory of the Kinneret Limnological Laboratory of the IOLR for the phosphorus analyses; we thank the captain and crew of the R.V. Shikmona and R.V. Bat Galim for their dedicated work during the sampling campaigns.

## Conflict of interest

The authors declare that the research was conducted in the absence of any commercial or financial relationships that could be construed as a potential conflict of interest.

## References

- Abd-El Monsef, H., Smith, S. E., and Darwish, K. (2015). Impacts of the Aswan high dam after 50 years. *Water Resour. Manage.* 29, 1873–1885. doi: 10.1007/s11269-015-0916-z
- Alvarez-Iglesias, P., Quintana, B., Rubio, B., and Pérez-Arlucca, M. (2007). Sedimentation rates and trace metal input history in intertidal sediments from San Simón Bay (Ría de Vigo, NW Spain) derived from  $^{210}\text{Pb}$  and  $^{137}\text{Cs}$  chronology. *J. Environ. Radioactivity* 98, 3 229–3 250. doi: 10.1016/j.jenvrad.2007.05.001
- Alve, E., Korsun, S., Schönfeld, J., Dijkstra, N., Golikova, E., Hess, S., et al. (2016). ForAM-AMBI: a sensitivity index based on benthic foraminiferal faunas from North-East Atlantic and Arctic fjords, continental shelves and slopes. *Mar. Micropaleontology* 122, 1–12. doi: 10.1016/j.marmicro.2015.11.001
- Avnaim-Katav, S., Almogi-Labin, A., Herut, B., Kanari, M., and Guy-Haim, T. (2021). Benthic foraminifera from the Southeastern Mediterranean shelf: Dead assemblages and living-dead comparisons recording consequences of Nile River damming. *Mar. Micropaleontology* 164, 101977. doi: 10.1016/j.marmicro.2021.101977
- Avnaim-Katav, S., Almogi-Labin, A., Kanari, M., and Herut, B. (2020). Living benthic foraminifera of southeastern Mediterranean ultra-oligotrophic shelf habitats: implications for ecological studies. *Estuarine Coast. Shelf Sci.* 234, 106633. doi: 10.1016/j.jess.2020.106633
- Avnaim-Katav, S., Almogi-Labin, A., Schneider-Mor, A., Crouvi, O., Burke, A. A., Kremenetski, K. V., et al. (2019). A multi-proxy shallow marine record for mid-to-late holocene climate variability, tephra eruptions and cultural change in the Eastern Mediterranean. *J. Quaternary Sci. Rev.* 204, 133–148. doi: 10.1016/j.quascirev.2018.12.001
- Best, J. (2019). Anthropogenic stresses on the world's big rivers. *Nat. Geosci.* 12 (1), 7–21. doi: 10.1038/s41561-018-0262-x
- Bookman, R., Mor-Federman, T., Herut, B., Harlavan, Y., Taha, N., Stein, M., et al. (2021). Development of the Nile Littoral Cell during the past 8.2 kyr. *Quaternary Sci. Rev.* 274, 107262. doi: 10.1016/j.quascirev.2021.107262
- Bouchet, V. M. P., Frontalini, F., Francescangeli, F., Sauriau, P.-G., Geslin, E., Martins, M. V. A., et al. (2021). Indicative value of benthic foraminifera for biomonitoring: Assignment to ecological groups of sensitivity to total organic carbon of species from European intertidal areas and transitional waters. *Mar. pollut. Bull.* 164, 112071. doi: 10.1016/j.marpolbul.2021.112071
- Bouchet, V. M. P., Goberville, E., and Frontalini, F. (2018). Benthic foraminifera to assess the Ecological Quality Status of Italian transitional waters. *Ecol. Indic.* 84, 130–139. doi: 10.1016/j.ecolind.2017.07.055
- Cimerman, F., and Langer, M. R. (1991). Mediterranean foraminifera. *Academia scientiarum et artium slovenica, dela, opera* 30, classis IV. *Hist. Nat.*, 118 p., 93 pl.
- Clarke, K. R. (1993). Non-parametric multivariate analyses of changes in community structure. *Aust. J. Ecol.* 18 (1), 117–143. doi: 10.1111/j.1442-9993.1993.tb00438.x
- Crouvi, O., Amit, R., Enzel, Y., Porat, N., and Sandler, A. (2008). Sand dunes as a major proximal dust source for late Pleistocene loess in the Negev desert, Israel. *Quaternary Res.* 70, 275–282. doi: 10.1016/j.yqres.2008.04.011
- Dethier, E. N., Renshaw, C. E., and Magilligan, F. J. (2022). Rapid changes to global river suspended sediment flux by humans. *Science* 376 (6600), 1447–1452.
- Dowidar, N. M. (1984). Phytoplankton biomass and primary productivity of the south-eastern Mediterranean. *Deep Sea Res. Part A. Oceanographic Res. Papers* 31 (6–8), 983–1000. doi: 10.1016/0198-0149(84)90052-9

## Publisher's note

All claims expressed in this article are solely those of the authors and do not necessarily represent those of their affiliated organizations, or those of the publisher, the editors and the reviewers. Any product that may be evaluated in this article, or claim that may be made by its manufacturer, is not guaranteed or endorsed by the publisher.

## Supplementary material

The Supplementary Material for this article can be found online at: <https://www.frontiersin.org/articles/10.3389/fmars.2023.1226379/full#supplementary-material>

Eckert, W., Didenko, J., Uri, E., et al. (2003). Spatial and temporal variability of particulate phosphorus fractions in seston and sediments of Lake Kinneret under changing loading scenario. In: Kronvang, B. (eds) *The Interactions between Sediments and Water. Developments in Hydrobiology*, vol 169. Springer, Dordrecht. doi: 10.1007/978-94-017-3366-3\_30

Farhat, H. I., and Salem, S. G. (2015). Effect of flooding on distribution and mode of transportation of Lake Nasser sediments, Egypt. *Egyptian J. Aquat. Res.* 41 (2), 165–176. doi: 10.1016/j.ejar.2015.03.009

Frihy, O. E. (1988). Nile Delta shoreline changes: aerial photographic study of a 28-year period. *J. Coast. Res.*, 597–606.

Frihy, O. E., and Komar, P. D. (1991). Patterns of beach-sand sorting and shoreline erosion on the Nile Delta. *J. Sedimentary Res.* 61 (4), 544–550.

Frihy, O. E., and Lotfy, M. F. (1997). Shoreline changes and beach-sand sorting along the northern Sinai coast of Egypt. *Geo-Marine Lett.* 17, 140–146. doi: 10.1007/s003670050019

Goericke, R., and Fry, B. (1994). Variations of marine plankton  $\delta^{13}\text{C}$  with latitude, temperature, and dissolved  $\text{CO}_2$  in the world ocean. *Global Biogeochemical Cycles* 8 (1), 85–90. doi: 10.1029/93GB03272

Goineau, A., Fontanier, C., Mojtahid, M., Fanget, A. S., Bassetti, M. A., and Jorissen, F. J. (2015). Live-dead comparison of benthic foraminiferal faunas from the Rh $\delta$ one prodelta (Gulf of Lions, NW Mediterranean): Development of a proxy for palaeoenvironmental reconstructions. *Mar. Micropaleontology* 119, 17–33. doi: 10.1016/j.marmicro.2015.07.002

Halim, Y. (1960). Observations on the Nile bloom of phytoplankton in the Mediterranean. *ICES Journal of Marine Science* 26, 1, 57–67. doi: 10.1093/icesjms/26.1.57

Halim, Y., Morcos, S. A., Rizkalla, S., and El-Sayed, M. K. (1995). "The impact of the Nile and the Suez Canal on the living marine resources of the Egyptian Mediterranean waters, (1958–1986)," in *Effects of riverine inputs on coastal ecosystems and fisheries resources*, vol. 349, p. 19–56.

Harmelin-Vivien, M., Loizeau, V., Mellon, C., Beker, B., Arlhac, D., Bodiguel, X., Bodiguel, X., et al. (2008). Comparison of C and N stable isotope ratios between surface particulate organic matter and microphytoplankton in the Gulf of Lions (NW Mediterranean). *Continental Shelf Res.* 28 (15), 1911–1919. doi: 10.1016/j.csr.2008.03.002

Hayward, B. W., Sabaa, A. T., and Triggs, C. M. (2019). Using foraminiferal test-size distribution and other methods to recognize Quaternary bathyal turbidites and taphonomically-modified faunas. *Mar. Micropaleontology* 148, 65–77. doi: 10.1016/j.marmicro.2019.03.008

Hecht, A. (1964). *On the turbulent diffusion of the water of the Nile floods in the Mediterranean Sea* Vol. 36 (Haifa, Israel: Sea Fisheries Research Station, Bulletin), 1–24.

Hecht, A., and Gertman, I. (2001). Physical features of the eastern Mediterranean resulting from the integration of POEM data with Russian Mediterranean cruises. *Deep Sea Res. Part I. Oceanographic Res. Papers* 48 (8), 1847–1876. doi: 10.1016/S0967-0637(00)00113-8

Hedges, J. I., Keil, R. G., and Benner, R. (1997). What happens to terrestrial organic matter in the ocean? *Organic geochemistry* 27 (5–6), 195–212. doi: 10.1016/S0146-6380(97)00066-1

- Hedges, J. I., and Oades, J. M. (1997). Comparative organic geochemistries of soils and marine sediments. *Organic geochemistry* 27 (7-8), 319–361. doi: 10.1016/S0146-6380(97)00056-9
- Herut, B., Almogi-Labin, A., Jannink, N., and Gertman, I. (2000). The seasonal dynamics of nutrient and chlorophyll a concentrations on the SE Mediterranean shelf-slope. *Oceanologica Acta* 23 (7), 771–782. doi: 10.1016/S0399-1784(00)01118-X
- Hottinger, L., Halicz, E., and Reiss, Z. (1993). *Recent foraminifera from the gulf of aqaba, red sea*, 33 (Ljubljana: Opera Sazu), 179 p., 230 pls.
- Hyams-Kaphzan, O., Almogi-Labin, A., Sivan, D., and Benjamini, C. (2008). Benthic foraminifera assemblage change along the southeastern Mediterranean inner shelf due to fall-off of Nile-derived siliciclastics. *Neues Jahrbuch für Geologie und Paläontologie-Abhandlungen* 248, 315–344. doi: 10.1127/0077-7749/2008/0248-0315
- Inman, D. L. (2003). Littoral cells.
- Inman, D. L., Elwany, M. H. S., Khafagy, A. A., and Golik, A. (1993). “Nile Delta profiles and migrating sand blankets,” in *Coastal engineering 1992*, 3273–3284.
- Inman, D. L., and Jenkins, S. A. (1984). “The Nile littoral cell and man’s impact on the coastal littoral zone in the SE Mediterranean,” in *Proceedings of the 17th International Coastal Engineering Conference*. 1600–1617 (Australia: ASCE, Sydney).
- Jones, R. W. (1994). *The challenger foraminifera* (London: Oxford University Press. Natural History Museum Pub.), 149 pp., 115 pls.
- Jorissen, F. J., de Stigter, H. C., and Widmark, J. G. V. (1995). A conceptual model explaining benthic foraminiferal microhabitats. *Mar. micropaleontology* 26 (1-4), 3–15. doi: 10.1016/0377-8398(95)00047-X
- Jorissen, F., Nardelli, M. P., Almogi-Labin, A., Barras, C., Bergamin, L., Bicchi, E., et al. (2018). Developing Foraminiferal Bioindex (FBI) for biomonitoring in the Mediterranean: species assignments to ecological categories. *Mar. Micropaleontology* 140, 33–45. doi: 10.1016/j.marmicro.2017.12.006
- Katz, M. E., Cramer, B. S., Franzese, A., Hönisch, B., Miller, K. G., Rosenthal, Y., et al. (2010). Traditional and emerging geochemical proxies in foraminifera. *J. Foraminiferal Res.* 40 (2), 165–192. doi: 10.2113/gsfjr.40.2.165
- Kidwell, S. M. (2007). Discordance between living and death assemblages as evidence for anthropogenic ecological change. *PNAS* 104, 17701–17706. doi: 10.1073/pnas.0707194104
- Kirchner, G., and Ehlers, H. (1998). Sediment geochronology in changing coastal environments: potentials and limitations of the <sup>137</sup>Cs and <sup>210</sup>Pb methods. *J. Coast. Res.* 14 (2), 483–492.
- Klein, M. (2000). The formation and disappearance of a delta at the El-Arish river mouth. IAHS PUBLICATION, 303–310.
- Kolde, R., and Maintainer, R. K. (2018). *Package 'pheatmap*, Vol. 1. 10, R package.
- Kress, N., Rahav, E., Silverman, J., and Herut, B. (2019). Environmental status of Israel’s Mediterranean coastal waters: Setting reference conditions and thresholds for nutrients, chlorophyll-a and suspended particulate matter. *Mar. pollut. Bull.* 141, 612–620. doi: 10.1016/j.marpolbul.2019.02.070
- Krom, M. D., Cliff, R. A., Eijssink, L. M., Herut, B., and Chester, R. (1999). The characterisation of Saharan dusts and Nile particulate matter in surface sediments from the Levantine basin using Sr isotopes. *Mar. Geology* 155 (3-4), 319–330. doi: 10.1016/S0025-3227(98)00130-3
- Li, D., Lu, X., Overeem, I., Walling, D. E., Syvitski, J., Kettner, A. J., et al. (2021). Exceptional increases in fluvial sediment fluxes in a warmer and wetter High Mountain Asia. *Science* 374 (6567), 599–603.
- Li, Y., Zhang, H., Tu, C., Fu, C., Xue, Y., and Luo, Y. (2016). Sources and fate of organic carbon and nitrogen from land to ocean: Identified by coupling stable isotopes with C/N ratio. *Estuarine Coast. Shelf Sci.* 181, 114–122. doi: 10.1016/j.ecss.2016.08.024
- Loeblich, A. R., and Tappan, H. (1987). *Foraminiferal genera and their classification*, 2 (New York: Van Nostrand Reinhold Company), 970 pp. 847 pls.
- Loeblich, A. R., and Tappan, H. (1994). *Foraminifera of the sahal shelf and timor sea* (Cushman Foundation for Foraminiferal Research), 661 pp. 393 pls. Special Publication No. 31.
- Ludwig, W., Dumont, E., Meybeck, M., and Heussner, S. (2009). River discharges of water and nutrients to the Mediterranean and Black Sea: major drivers for ecosystem changes during past and future decades? *Prog. oceanography* 80 (3-4), 199–217. doi: 10.1016/j.pocean.2009.02.001
- Magill, C. R., Ausin, B., Wenk, P., McIntyre, C., Skinner, L., Martínez-García, A., et al. (2018). Transient hydrodynamic effects influence organic carbon signatures in marine sediments. *Nat. Commun.* 9 (1), 4690. doi: 10.1038/s41467-018-06973-w
- Martinez, T., Marchant, M., and Urbina, M. (2023). Are physiological responses in foraminifera reliable environmental stress bioindicators? *A systematic review. Environ. Res.* 216 (Part 2), 114515. doi: 10.1016/j.envres.2022.114515
- Meyers, P. A. (1994). Preservation of elemental and isotopic source identification of sedimentary organic matter. *Chem. geology* 114 (3-4), 289–302. doi: 10.1016/0009-2541(94)90059-0
- Milliman, J. D., and Farnsworth, K. L. (2013). *River discharge to the coastal ocean: a global synthesis* (Cambridge University Press).
- Mushkin, A., Katz, O., Crouvi, O., Alter, S. R., and Shemesh, R. (2016). Sediment contribution from Israel’s coastal cliffs into the Nile’s littoral cell and its significance to cliff-retreat mitigation efforts. *Eng. Geology* 215, 91–94. doi: 10.1016/j.enggeo.2016.11.005
- Nir, Y. (1984). Recent sediments of the Israel Mediterranean continental shelf and slope (Sweden: Göteborg University), 149 pp. (PhD Dissertation).
- Nixon, S. W. (2003). Replacing the Nile: are anthropogenic nutrients providing the fertility once brought to the Mediterranean by a great river? *AMBIO: A J. Hum. Environ.* 32 (1), 30–39. doi: 10.1579/0044-7447-32.1.30
- Oksanen, J. F., et al. (2019) *vegan: Community ecology package*. Available at: <https://CRAN.R-project.org/package=vegan>.
- Oren, O. H. (1969). Oceanographic and biological influence of the Suez Canal, the Nile and the Aswan Dam on the Levant Basin. *Prog. Oceanography* 5, 161–167. doi: 10.1016/0079-6611(69)90038-X
- Oren, O. H., and Komarovskiy, B. (1961). The influence of the Nile flood on the shore waters of Israel. *Rapports et Proces-Verbaux des Reunions, Conseil International pour l’Exploration Scientifique de la Mer Medeterranee. Monaco* 16, 655–659.
- Ozer, T., Gertman, I., and Gildor H and Herut, B. (2022). Thermohaline temporal variability of the SE mediterranean coastal waters (Israel) – long-term trends, seasonality, and connectivity. *Front. Mar. Sci.* 8. doi: 10.3389/fmars.2021.799457
- Ransby, D., Fischer, H. W., Herut, B., and Almogi-Labin, A. Radionuclides and chronology of short sediment cores BY and ASH from the Israel inner Mediterranean shelf. *PANGAEA*. doi: 10.1594/PANGAEA.956901
- Reale, M., Cossarini, G., Lazzari, P., Lovato, T., Bolzon, G., Masina, S., et al. (2022). Acidification, deoxygenation, and nutrient and biomass declines in a warming Mediterranean Sea. *Biogeosciences* 19 (17), 4035–4065. doi: 10.5194/bg-19-4035-2022
- Richon, C., Dutay, J. C., Bopp, L., Le Vu, B., Orr, J. C., Somot, S., et al. (2019). Biogeochemical response of the Mediterranean Sea to the transient SRES-A2 climate change scenario. *Biogeosciences* 16 (1), 135–165. doi: 10.5194/bg-16-135-2019
- Rohling, E. J., Marino, G., and Grant, K. M. (2015). Mediterranean climate and oceanography, and the periodic development of anoxic events (sapropels). *Earth-Science Rev.* 143, 62–97. doi: 10.1016/j.earscirev.2015.01.008
- Schmiedl, G. (2019). “Use of foraminifera in climate science,” in *Oxford research encyclopedia of climate science* (Oxford University Press). doi: 10.1093/acrefore/9780190228620.013.735
- Schonfeld, J., Alve, E., Geslin, E., Jorissen, F., Korsun, S., Spezzaferri, S., et al. (2012). The FOBIMO (Foraminiferal Bio-Monitoring) initiative—towards a standardized protocol for soft-bottom benthic foraminiferal monitoring studies. *Mar. Micropaleontology* 94, 1–13. doi: 10.1016/j.marmicro.2012.06.001
- Sen Gupta, B. K. (Ed.) (1999). *Modern foraminifera* (Dordrecht, the Netherlands: Kluwer Academic Publishers).
- Shaeri, S., Etemad-Shahidi, A., and Tomlinson, R. (2020). Revisiting longshore sediment transport formulas. *J. Waterway Port Coastal Ocean Eng.* 146 (4), 04020009. doi: 10.1061/(ASCE)WW.1943-5460.0000557
- Sharaf El Din, S. H. (1977). Effect of the Aswan High Dam on the Nile flood and on the estuarine and coastal circulation pattern along the Mediterranean Egyptian coast. *Limnology Oceanography* 22 (2), 194–207. doi: 10.4319/lo.1977.22.2.0194
- Shultz, D. J., and Calder, J. A. (1976). Organic carbon <sup>13</sup>C<sup>12</sup>C variations in estuarine sediments. *Geochimica Cosmochimica Acta* 40 (4), 381–385. doi: 10.1016/0016-7037(76)90002-8
- Singh, W., Hjørleifsson, E., and Stefansson, G. (2011). Robustness of fish assemblages derived from three hierarchical agglomerative clustering algorithms performed on Icelandic groundfish survey data. *ICES J. Mar. Sci.* 68 (1), 189–200. doi: 10.1093/icesjms/fsq144
- Smith, S. E., and Abdel-Kader, A. (1988). Coastal erosion along the Egyptian delta. *J. Coast. Res.*, 245–255.
- Stanley, D. J., and Warne, A. G. (1993). Nile Delta: recent geological evolution and human impact. *Science* 260 (5108), 628–634.
- Syvitski, J. P. M., Vörösmarty, C. J., Kettner, A. J., and Green, P. (2005). Impact of humans on the flux of terrestrial sediment to the global coastal ocean. *Science* 308 (5720), 376–380. doi: 10.1126/science.1109454.
- Van Wellen, E., Chadwick, A. J., and Mason, T. (2000). A review and assessment of longshore sediment transport equations for coarse-grained beaches. *Coast. Eng.* 40 (3), 243–275. doi: 10.1016/S0378-3839(00)00031-4
- Vörösmarty, C. J., Meybeck, M., Fekete, B., Sharma, K., Green, P., and Syvitski, J. P. (2003). Anthropogenic sediment retention: major global impact from registered river impoundments. *Global Planetary Change* 39 (1-2), 169–190. doi: 10.1016/S0921-8181(03)00023-7
- Wheeler, K. G., Jeuland, M., Hall, J. W., Zagona, E., and Whittington, D. (2020). Understanding and managing new risks on the Nile with the Grand Ethiopian Renaissance Dam. *Nat. Commun.* 11 (1), 5222. doi: 10.1038/s41467-020-19089-x
- Woodward, J. C., Macklin, M. G., Krom, M. D., Williams, M. A., and Gupta, A. (2007). The Nile: evolution, Quaternary river environments and material fluxes. *Large rivers: geomorphology Manage.* 13, 712.
- WoRMS Editorial Board (2023) *WoRMS editorial board world register of marine species*. Available at: <https://www.marinespecies.org> (Accessed 2023-02-09). at VLIZ.
- Zviely, D., Kit, E., and Klein, M. (2007). Longshore sand transport estimates along the Mediterranean coast of Israel in the Holocene. *Mar. Geology* 238 (1-4), 61–73. doi: 10.1016/j.margeo.2006.12.003